

# Geophysical Research Letters

## RESEARCH LETTER

10.1029/2018GL081788

### Key Points:

- Moderate shoaling of winter mixed layer causes increase in primary production, but shoaling below a threshold depth can lead to a collapse
- Reversal in this response is due to balancing effects of iron and light limitation and associated with a change in community structure and export efficiency
- Interestingly, shoaling summer mixed layer always reduces PP and export because of a reduction of the productive volume

### Correspondence to:

J. Llorc,  
jllorc@utas.edu.au

### Citation:

Llorc, J., Lévy, M., Sallée, J. B., & Tagliabue, A. (2019). Nonmonotonic response of primary production and export to changes in mixed-layer depth in the Southern Ocean. *Geophysical Research Letters*, 46, 3368–3377. <https://doi.org/10.1029/2018GL081788>




Received 20 DEC 2018

Accepted 12 MAR 2019

Accepted article online 18 MAR 2019

Published online 29 MAR 2019

## Nonmonotonic Response of Primary Production and Export to Changes in Mixed-Layer Depth in the Southern Ocean

J. Llorc<sup>1,2</sup> , M. Lévy<sup>3</sup> , J. B. Sallée<sup>3</sup>, and A. Tagliabue<sup>4</sup> 

<sup>1</sup>Institute of Marine and Antarctic Studies, University of Tasmania, Hobart, Tasmania, Australia, <sup>2</sup>Centre of Excellence for Climate System Science, Australian Research Council, Hobart, Tasmania, Australia, <sup>3</sup>Sorbonne Université, LOCEAN-IPSL, CNRS/IRD/MNHN, Paris, France, <sup>4</sup>School of Environmental Sciences, University of Liverpool, Liverpool, UK

**Abstract** Ongoing and future changes in wind and temperature are predicted to alter upper ocean vertical mixing across the Southern Ocean. How these changes will affect primary production (PP) remains unclear as mixing influences the two controlling factors: light and iron. We used a large ensemble of 1-D-biogeochemical model simulations to explore the impacts of changes in mixed-layer depths on PP in the Southern Ocean. In summer, shoaling mixed-layer depth always reduced depth-integrated PP, despite increasing production rates. In winter, shoaling mixed layers had a two-staged impact: for moderate shoaling PP increased as light conditions improved, but more pronounced shoaling decreased iron supply, which reduced PP. The fraction of PP exported below 100 m also presented a nonmonotonic behavior. This suggests a potential future shift from a situation where reduced winter mixing increases PP and export, to a situation where PP and export may collapse if the ML shoals above a threshold depth.

**Plain Language Summary** In the Southern Ocean, atmospheric warming associated to climate change is altering the depth at which surface waters are stirred, the so-called mixed-layer depth. A change in the mixed-layer depth impacts the phytoplankton cells that inhabit it by altering their two main limiting factors: iron and light. However, the sign and magnitude of this impact are still not clear. In this work we used mathematical simulations to explain how changes in the seasonal mixed-layer depth modify the supply of iron and the amount of light, and how these changes impact phytoplankton activity. Our results show that mixed-layer depth changes in summer and in winter have different impacts. Reducing summer mixed-layer depth did not change the iron supply, but it reduced the volume of water where phytoplankton thrived. In winter, shallower mixed-layer depth altered iron and light but in opposed ways. At first, phytoplankton increased its activity as more light became available. However, a continued shallowing of the mixed-layer depth eventually reduced the iron supply and the phytoplankton activity. Our study proposes a new interpretation on how ongoing changes in the Southern Ocean impact phytoplankton activity and alerts of the presence of threshold depths for the winter mixed layer above which phytoplankton may struggle to survive.

## 1. Introduction

Southern Ocean (SO) atmospheric and oceanic conditions are currently changing in response to increasing atmospheric concentrations of greenhouse gases and changes in the concentration of stratospheric ozone (Swart et al., 2018). Model projections from the fifth phase of the Coupled Model Intercomparison Project (CMIP5; Taylor et al., 2012) highlight a changing wind pattern associated with a more persistent phase of the Southern Annular Mode (SAM), together with warmer sea-surface temperature north of the sea ice zone (Bracegirdle et al., 2013; Cai et al., 2005; Swart et al., 2015; Zheng et al., 2013). Such changes in the physical environment are expected to affect the capacity of phytoplankton to fix atmospheric carbon, their community composition, and the overall efficiency of the biological carbon pump (Lenton & Mearns, 2007; Lovenduski & Gruber, 2005). In particular, it is critical to understand how physical changes will alter iron and light availability, as these two elements play fundamental roles in structuring the response of phytoplankton communities (Boyd et al., 2010).

In a recent review, Deppeler and Davidson (2017) identified a large number of factors able to alter primary production (PP) in the SO. Among these factors, changes in the seasonal mixed-layer depth (MLD) were

particularly important north of the sea ice zone. However, neither the sign nor the magnitude of change is yet clear due to the complex links between the seasonal cycle of the MLD and PP in the SO. Two reasons contribute to this complexity. First, the sign of the change in MLD is expected to vary regionally and seasonally, depending on changes in surface warming, wind, and freshwater fluxes (Panassa et al., 2018; Sallée et al., 2013). Second, vertical mixing plays a complex role for phytoplankton, since shallow MLDs may maintain cells in the well-lit part of the water column, but, at the same time, the vertical extent of the upper mixing layer controls the vertical supply of iron from deeper reserves. Thus, while a decrease in MLD enhances productivity in light limited conditions through the first mechanism, it reduces productivity through the second mechanism in regions where iron is supplied by vertical mixing in winter (Doney, 2006; Sarmiento et al., 2004). In this second case, the winter supply of iron is more efficient when the mixed-layer deepens within the subsurface iron reservoir (hereafter, we refer to the upper limit of the iron reservoir as the ferricline, see methods for details). The two mechanisms described by this paradigm are concomitant in the SO, where both light limitation and iron limitation coexist in time and space (Boyd et al., 2010). Moreover, given that such interplay varies throughout the seasonal cycle, changes in the seasonal extremes of the MLD in winter and summer ( $MLD_{\text{winter}}$  and  $MLD_{\text{summer}}$ , respectively) are expected to have different impacts on annual values of PP (Deppeler & Davidson, 2017; Hauck et al., 2015).

End-of-century projections from CMIP5 show a coherent latitudinal pattern of change in PP over the SO (Bopp et al., 2013; Laufkötter et al., 2015). In the 30–40°S latitudinal band CMIP5 models agree on a nutrient-driven decrease in PP as a consequence of the broadening of oligotrophic gyres to southern waters (Hauck et al., 2015). In the 40–50°S latitudinal band, models project an increase in PP, followed by a decrease in the 50–65°S band (Bopp et al., 2013). Leung et al. (2015) found a consistent response between models on the PP increase at 40–50°S. Their analysis associated the change in PP to a reduction of  $MLD_{\text{summer}}$  combined with an increase in surface iron. Alternatively, the PP decrease in the 50–65°S band was not consistent between models and has been linked to deeper  $MLD_{\text{summer}}$  combined with a reduction of the incident photosynthetically available radiation. However, the mechanisms behind these changes remain unclear as projected patterns have only been explained through correlation relationships (Leung et al., 2015) or masked by the strong PP increase associated to Antarctic sea ice decline (Laufkötter et al., 2015). The overlap between different drivers in climate models does not allow evaluating the influence of changes in MLD alone over PP. Furthermore, the uncertainties in these models are likely to induce incorrect interpretations based on theoretical paradigms (Lovenduski & Gruber, 2005). The largest uncertainty is caused by the inability of CMIP5 models to correctly reproduce dissolved iron and MLD observations in the SO (Sallée et al., 2013; Tagliabue et al., 2016), particularly in winter. These uncertainties cascade into the iron vertical supply and cause a model-dependent biogeochemical response in the SO (Schourup-Kristensen, 2015).

Moreover, the lack of mechanistic understanding and the uncertainties associated to PP drivers in the SO also impact the estimates of how much carbon is eventually transferred into the deep ocean. The export of carbon depends on a number of processes such as the plankton community structure, remineralization rates, temperature, or MLD variability (Boyd & Trull, 2007; Henson et al., 2015). The disparities on how biogeochemical models resolve these mechanisms add up to iron supply uncertainties and cause a lack of agreement between climate-models in the SO (Laufkötter et al., 2016). This lack of consensus is particularly severe in the midlatitudes, 44–58°S (Hauck et al., 2015).

A number of observation-based studies provide evidences that in the SO the two aspects of the PP-MLD paradigm (Figure 1 in Doney, 2006) might be occurring simultaneously. Ardyna et al. (2017) combined data from satellite ocean-color with Argo floats to show that regional variability in SO phytoplankton biomass results from a mixed balance of drivers in addition to light, including the proximity to island or submerged seamounts, sea ice, or  $MLD_{\text{winter}}$ . Interestingly, they show that away from specific iron sources, phytoplankton biomass increases as a function of  $MLD_{\text{winter}}$ , for  $MLD_{\text{winter}}$  ranging from 0 to ~150 m, but decreases for  $MLD_{\text{winter}} > 150$  m. They interpret the presence of such a regime shift as a transition from an iron-limited environment (shallow  $MLD_{\text{winter}}$ ) to a light-limited environment (deep  $MLD_{\text{winter}}$ ). Similarly, Hoppe et al. (2017) reported strong blooming conditions in regions of deep mixing, suggesting a secondary role of light limitation on controlling summer production. This result agrees with Venables and Moore (2010), who found no influence of light limitation over the annual integrated chlorophyll-a in SO waters.

In this paper, we investigate how ongoing and future changes in winter and summer MLD may influence PP and the export of organic carbon with a modeling configuration specifically designed to address this question in the context of the SO. Our approach avoids the complexity related to climate models and, at the same time, captures the double-role of the MLD on PP. To do so, we implemented a state-of-the-art biogeochemical model into a fully controlled one-dimensional (1-D) physical configuration. We varied  $MLD_{winter}$ ,  $MLD_{summer}$ , and ferricline depth ( $Z_{Fe}$ ) along typical present and projected ranges for the SO. Despite the idealized approach, the statistical analysis of a large ensemble (752) of simulated annual cycles showed a complex relationship between MLD, PP, and export. Our results challenge current interpretations of CMIP5 projections in the SO and propose the presence of a threshold depth for  $MLD_{winter}$  below which production would collapse.

## 2. Methods

### 2.1. Model Configuration

Our model configuration represents an ocean water column resolved as a vertical grid of 75 equally spaced cells. Only vertical exchanges are considered (i.e., it is a 1-D configuration). The same configuration was used in Llort et al. (2015) to study the bloom phenology in the SO and is fully described therein; here we recall the fundamental model characteristics. We use the biogeochemical model PISCES (Aumont & Bopp, 2006) that we force with three physical variables: surface solar short-wave radiation, temperature, and turbulent vertical mixing ( $\kappa_z$ ). These three variables are prescribed and follow a complete seasonal cycle starting on 15 February. The vertical profile of  $\kappa_z$  is set as a step-like function, with a value of  $1 \text{ m}^2/\text{s}$  within an upper mixed layer and a small open ocean mixing of  $10^{-5} \text{ m}^2/\text{s}$  (Cisewski et al., 2005) below the mixed layer. The strong mixing in the upper layer ensures a homogenous vertical distribution of phytoplankton and nutrients (Lévy, 2015). The depth of the surface mixed layer (and thus the penetration depth of strong vertical mixing) varies along an idealized seasonal cycle consisting of three phases (Figures 1a and 1b): a first phase of linear deepening until the maximum depth ( $MLD_{winter}$ , from 15 February to 15 September), a second phase of linear shoaling (from 15 September to 15 December), and a period of constant depth in summer ( $MLD_{summer}$ , 15 December to 14 February of the next year).

PISCES contains 24 biogeochemical tracers, among which five nutrients (nitrate, phosphate, ammonium, iron, and silicate), two phytoplankton size classes (small and large), and two zooplankton size classes (microzooplankton and mesozooplankton). Large phytoplankton differs from small phytoplankton by higher iron requirements and a greater iron half-saturation constant.

Initial vertical profiles for macronutrient (i.e., nitrate, phosphate, and silicate) were constructed based on the winter mean profiles of a typical HNLC region (Jeandel et al., 1998). We carried a series of sensitivity experiments to ensure that only iron limits phytoplankton growth. The summer initial condition for dissolved iron profile was constructed by assuming low concentrations ( $0.03 \text{ nmol Fe/L}$ ) above a prescribed depth and larger concentrations ( $0.5 \text{ nmol Fe/L}$ ) below. The depth where iron concentration suddenly increases is referred here as the ferricline ( $Z_{Fe}$ ). Iron supply into the upper mixed layer is not prescribed but emerges from the vertical entrainment and diffusion of iron, which depends on the respective depth of the  $Z_{Fe}$  and the MLD. While lateral advection might be another important source of dissolved iron in specific SO regions, particularly in the lee of islands or continental shelves, it is neglected here to concentrate on vertical entrainment of iron. Vertical entrainment of iron is likely the dominant source of iron supply in most of the SO, which is characterized by deep ferricline (Tagliabue et al., 2014). In this study, iron supply is computed as the amount of dissolved iron that enters MLD.

### 2.2. Ensemble of Runs

The 1-D physical setting forced the PISCES model under current and future MLD conditions. We conducted an ensemble of simulations where we varied three forcing parameters,  $MLD_{winter}$ ,  $MLD_{summer}$  (Pellichero et al., 2017), and  $Z_{Fe}$  (Tagliabue et al., 2012), over the full range of observed values in the SO. Values for future MLD were obtained from CMIP5 climate model projections (Sallée et al., 2013; Taylor et al., 2012). Overall, we prescribed 11 distinct values of  $MLD_{winter}$  (between 100 and 600 m), combined with nine distinct values for  $MLD_{summer}$  (between 20 and 100 m) and eight  $Z_{Fe}$  values (between 150 and 500 m). The combination of all  $MLD_{winter}$ ,  $MLD_{summer}$ , and  $Z_{Fe}$  values resulted in 752 different

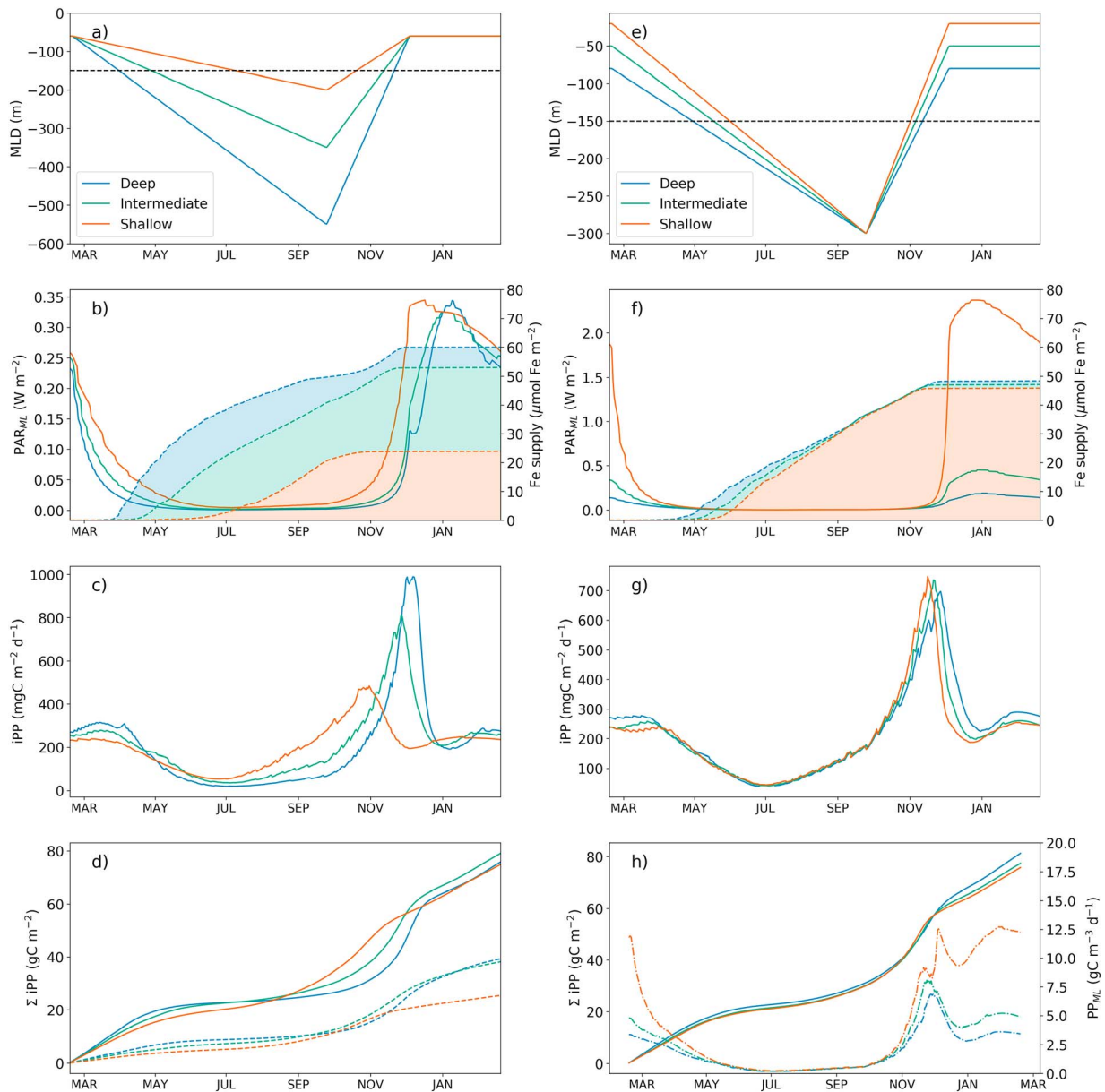


**Figure 1.** Left panels: Seasonal cycles of (a) mixed-layer depth, (b) averaged photosynthetically available radiation (PAR) in the mixed-layer depth (MLD; plain lines) and time-cumulative vertical supply of iron (dashed contours with colors filled) into the MLD, (c) depth-integrated primary production (iPP), and (d) time-cumulative integrated primary production ( $\Sigma iPP$ , plain lines) and integrated primary production for the large-phytoplankton group (dashed lines) for three simulations with identical  $Z_{Fe}$  depth and  $MLD_{summer}$  but with different  $MLD_{winter}$ . The black dashed line in (a) indicates the value of  $Z_{Fe}$ . Right panels: Same but for simulations runs with identical  $Z_{Fe}$  depth and  $MLD_{winter}$  and different  $MLD_{summer}$ . In (h), the dash-dotted lines represent primary production averaged in the mixed-layer ( $PP_{ML}$ ).

scenarios. This approach allowed us to identify how changes in MLD affect PP and export over a wide range of oceanic conditions typical of the SO.

### 3. Results

#### 3.1. Response to Changes in Winter MLD

SO open waters extend from midlatitude to high latitude, with seasons being clearly differentiated and incident photosynthetically available radiation (PAR) being lower in winter than in summer. However, the average light received by phytoplankton is lower than surface PAR as cells are vertically mixed across the mixed

layer. The light used for the photosynthesis can then be calculated using the PAR attenuation profile averaged across the mixed layer ( $PAR_{ML}$ ). Thus, deeper (shallower)  $MLD_{winter}$  reduce (increase)  $PAR_{ML}$ , exacerbating (relaxing) light limitation of phytoplankton growth and PP (Boyd et al., 2010).  $MLD_{winter}$  also has an impact on growth and PP limitation by controlling vertical supply of iron. Deeper  $MLD_{winter}$  tend to drive stronger iron supplies and enhance phytoplankton growth (Tagliabue et al., 2014). We first examine how the combination of these two opposing mechanisms (light and iron limitation) drive differences in PP in three model simulations that only differ by their  $MLD_{winter}$  values (deep, intermediate, and shallow scenario), with identical  $MLD_{summer}$  and  $Z_{Fe}$  (Figure 1, left panels).

From March to July, the seasonal decrease of surface PAR combined with the deepening of the mixed layer strongly decreased  $PAR_{ML}$  for all three scenarios (Figures 1a and 1b).  $PAR_{ML}$  remained low until October, when the shoaling of the MLD caused a rapid increase (Figure 1b). The vertical supply of iron initiated when the MLD crossed  $Z_{Fe}$  (Figure 1b). These two factors,  $PAR_{ML}$  and iron supply, acted together to shape the response in PP (Figures 1c and 1d). From March to July, depth-integrated PP was low and with a decreasing trend (Figure 1c). For the three scenarios a period of slow increase started around July and was followed by a marked bloom in spring.

The three simulations exhibited differences in the timing and amplitude of the bloom (Figure 1c). In the shallow simulation, winter iron supply was relatively low ( $24 \mu\text{mol Fe} \cdot \text{m}^{-2} \cdot \text{year}^{-1}$ ) and the bloom was the weakest and earliest. Production started increasing on 1 July and peaked in November, shortly after the mixing layer started shoaling and a month after iron supply ceased (Figures 1a–1c). On the contrary, the bloom in the deep  $MLD_{winter}$  simulation was the strongest and the slowest to develop of all three scenarios. In this scenario,  $MLD_{winter}$  penetrated deeply into  $Z_{Fe}$ , which enhanced the vertical flux of iron ( $60 \mu\text{mol Fe} \cdot \text{m}^{-2} \cdot \text{year}^{-1}$ ). Nevertheless, integrated PP did not increase until the mixed layer started shoaling in October. The large amount of accumulated iron during winter and the quick spring increase in  $PAR_{ML}$  supported a strong, but relatively short bloom, peaking in December.

Interestingly, these two extreme simulations led to similar values of annual integrated PP ( $74.8 \text{ g C m}^{-2} \cdot \text{year}^{-1}$  for the shallow simulation and  $75.5 \text{ g C} \cdot \text{m}^{-2} \cdot \text{year}^{-1}$  for the deep simulation; Figure 1d), yet the relative contributions of small and large phytoplankton were notably different. The annual PP supported by the large phytoplankton group represented 34% of the total production for the iron-poor shallow simulation while for the iron-rich deep simulation it reached 52% (dashed lines in Figure 1d).

When these two end-member simulations are compared to the intermediate  $MLD_{winter}$  scenario, a nonmonotonic response of annual PP to varying  $MLD_{winter}$  emerges. While the bloom in the intermediate  $MLD_{winter}$  simulation presented intermediate characteristics (iron supply was  $53 \mu\text{mol Fe} \cdot \text{m}^{-2} \cdot \text{year}^{-1}$ ; Figure 1c), it showed the highest annual production ( $79.1 \text{ g C} \cdot \text{m}^{-2} \cdot \text{year}^{-1}$ ) of all three simulations (Figure 1d). The balance between a weak, long-lasting and small-phytoplankton-dominated winter bloom and a high, quick and large-phytoplankton-dominated spring bloom appeared to be optimal in the case of the intermediate experiment.

When we analyzed the results from our ensemble of 752 simulations (Figure 2a), two contrasted modes emerged in the response of annual PP to changes in  $MLD_{winter}$ . The first mode was associated with a deep iron reservoir ( $Z_{Fe} > 350 \text{ m}$ ), and the second mode with a shallow iron reservoir ( $Z_{Fe} < 250 \text{ m}$ ). Both modes presented nonmonotonic PP- $MLD_{winter}$  relationships: for a given  $Z_{Fe}$ , PP increased as  $MLD_{winter}$  decreased, until  $MLD_{winter}$  reached a threshold depth ( $Z_{PPmax}$ , indicated by the white contours in Figure 2a), where the PP- $MLD_{winter}$  relationship reversed and PP started decreasing. The threshold depth marked a local maximum in PP and depended on the  $Z_{Fe}$  mode. Situations with  $250 \text{ m} < Z_{Fe} < 350 \text{ m}$  corresponded to a transition regime between these two modes, characterized by the presence of two  $Z_{PPmax}$  (dashed white lines in Figure 2a).

The deep iron reservoir mode presented a relatively shallow  $Z_{PPmax}$ , at around 200 m. In this mode, iron supplies were systemically low ( $< 10 \mu\text{mol Fe} \cdot \text{m}^{-2} \cdot \text{year}^{-1}$ ; black contours in Figure 2a), even when  $MLD_{winter}$  was deeper than  $Z_{Fe}$  since on those occasions there was only a brief period where MLD was deeper than  $Z_{Fe}$ . In contrast, the shallow  $Z_{Fe}$  mode was characterized by relatively large iron supplies, which were proportional to  $MLD_{winter}$ . In this mode, the threshold depths were deeper (between 350 and 500 m) and depended strongly on  $Z_{Fe}$ .

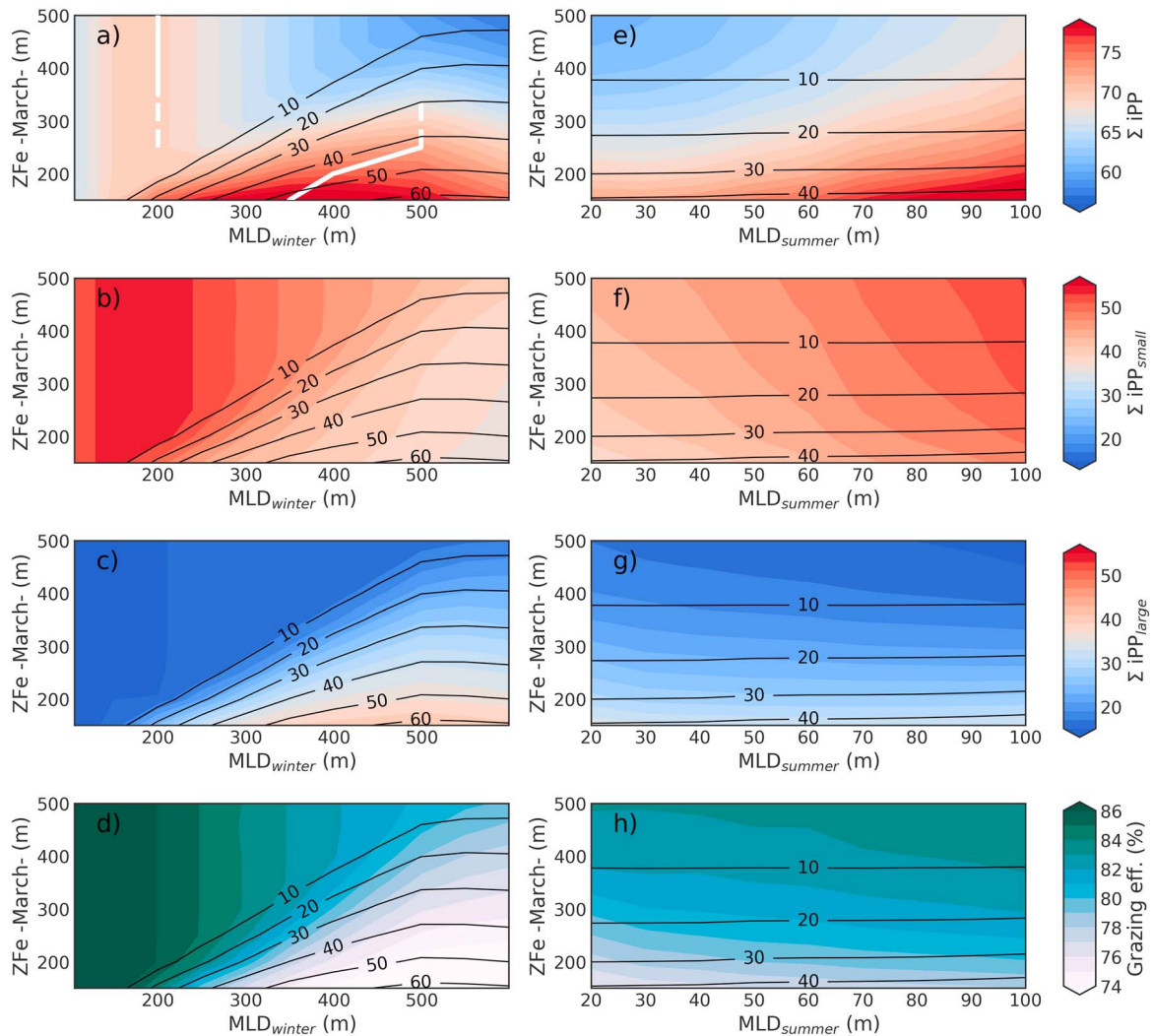


**Figure 2.** Left panels: (a) Annual integrated primary production (in  $\text{g C} \cdot \text{m}^{-2} \cdot \text{year}^{-1}$ ) as a function of initial ferricline depth ( $Z_{\text{Fe}}$ ) and winter mixed-layer depth (MLD;  $\text{MLD}_{\text{winter}}$ ). The white solid lines indicate threshold depths ( $Z_{\text{PPmax}}$ ), and the white dashed lines indicate the range where two different thresholds were detected. (b) Same as (a) but for small phytoplankton. (c) Same as (a) but for large phytoplankton. (d) Portion of annual primary production grazed by zooplankton (grazing efficiency). In all panels, the black contours show the vertical supply of iron ( $\text{nmolFe}/\text{year}$ ). Right panels: Same but against summer MLD ( $\text{MLD}_{\text{summer}}$ ).

In both modes, the iron supply and the contribution of the large phytoplankton group to total PP responded monotonically to changes in  $\text{MLD}_{\text{winter}}$ . This highlights that as for the example shown in Figure 1, the threshold depth of  $\text{MLD}_{\text{winter}}$  marks a boundary between two different community responses: for  $\text{MLD}_{\text{winter}}$  shallower than  $Z_{\text{PPmax}}$ , the community is dominated by small-phytoplankton, and PP of both large and small phytoplankton groups respond monotonically to changes in iron supply (Figures 2b and 2c); for  $\text{MLD}_{\text{winter}}$  deeper than  $Z_{\text{PPmax}}$ , the community is dominated by large-phytoplankton, and light becomes the dominant limiting factor, particularly for the small-phytoplankton group (Figure 2b).

The role of zooplankton in these responses was also addressed by diagnosing the percentage of PP grazed, hereinafter referred as the grazing efficiency. Our simulations show that grazing efficiency was strongly dependent on the community structure (Figure 2d), as small phytoplankton is more easily grazed than large phytoplankton. Such dependency suggests a minor role of zooplankton grazing as it follows the change on community structure, which is in turn caused by changes in MLD.

A further climate-relevant metric associated with marine production is how much of the organic carbon synthesized in the upper ocean is exported to the deep ocean. Under shallow ferricline conditions, the amount of production exported below 100 m (EP) showed a nonmonotonic response to changing

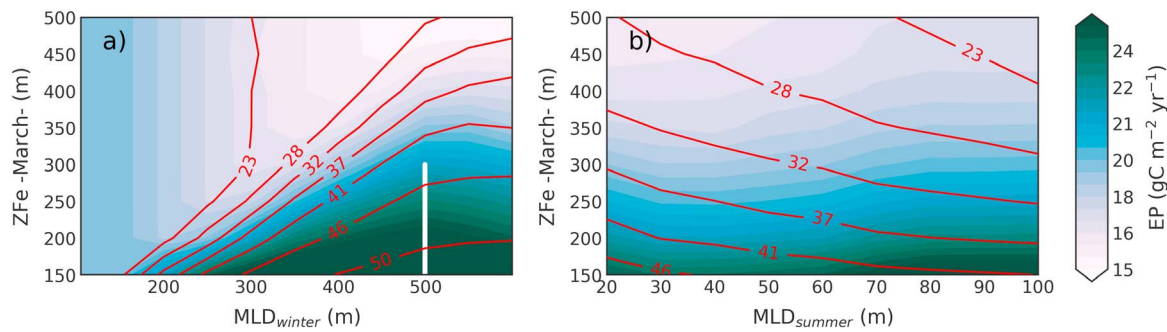


**Figure 3.** (a) Annual primary production exported below 100-m depth as a function of initial ferricline depth ( $Z_{Fe}$ ) and winter mixed-layer depth (MLD;  $MLD_{winter}$ ). The red contours show the percentage of primary production done by the large (and fast-sinking) phytoplankton. The white line indicates the threshold depth for EP-MLD relationship. (b) Same as (a) but against summer MLD ( $MLD_{summer}$ ).

$MLD_{winter}$  with a threshold depth at 500 m (Figure 3a). EP responded in parallel to the productivity supported by the larger class of phytoplankton (Figure 2c) because large phytoplankton tends to aggregate and sink faster than small phytoplankton (Boyd & Trull, 2007; Laufkötter et al., 2016). In contrast, and unlike PP, under deep ferricline and small phytoplankton conditions we observed a monotonic response, with a constant increase in export as  $MLD_{winter}$  decreased (Figure 3a).

### 3.2. Response to Changes in Summer MLD

Phytoplankton growth and PP rates are the highest during late spring and early summer as surface waters are replenished with iron and light is abundant (Boyd et al., 2010). Therefore, changes in  $MLD_{summer}$ , even if small in magnitude, have the potential to influence annual productivity (Laufkötter et al., 2015; Leung et al., 2015) and export (Hauck et al., 2015). In order to understand the mechanisms by which changes in  $MLD_{summer}$  affect PP, we first compared three simulations with different values of  $MLD_{summer}$  (20, 50, and 80 m) but with  $Z_{Fe}$  set to 150 m and  $MLD_{winter}$  at 300 m (Figure 1e). Dissolved iron supplies were very similar among the three simulations, but  $PAR_{ML}$  strongly differed, with values nine times larger in the shallow experiment than in the deep one (Figure 1f). Stronger light limitation in the deep experiment caused the bloom to be slightly weaker and last longer than in the shallow experiment (Figure 1g). However, annual PP was the largest in the deep experiment and this mainly resulted from an increase of the productive volume, which caused higher depth-integrated PP during summer (Figure 1h), despite having the lowest MLD-averaged production rates,  $PP_{ML}$  (dashed lines in Figure 1h).

The decrease in annual PP under shallower  $MLD_{summer}$  was consistent among all 752 simulations (Figure 2e). This response suggested that in our model annual PP was not light limited in summer.  $MLD_{summer}$  was always shallower than ferricline depths and iron supply remained low for all scenarios (black lines in Figures 2e–2g). Export production was less sensitive to changes in  $MLD_{summer}$  than PP (Figure 3b), due to the larger contribution of small phytoplankton cells to productivity under deep  $MLD_{summer}$  (Figure 2f).

## 4. Discussion and Conclusions

The analysis of our ensemble of model simulations revealed that changes in PP driven by changes in MLD are more complex than previously thought. The change in PP in response to variations in winter mixed layer was nonmonotonous: total PP and winter MLD were positively correlated for winter MLDs above a certain threshold depth (that we refer as  $Z_{PPmax}$ ) but negatively correlated for winter MLDs below this threshold (Figure 2a). The  $Z_{PPmax}$  for the mixed-layer emerged due to the overlap of the two limiting factors, light and iron availability (Figure 1b). Interestingly,  $Z_{PPmax}$  was related to both the biogeochemical conditions and ecosystem composition. For instance,  $Z_{PPmax}$  was shallower for iron-poor and small-phytoplankton dominated conditions than for iron-rich conditions where the two phytoplankton groups contributed more equally (Figure 2b). Our analysis also shown that quite unexpectedly, deeper summer mixed-layers induced larger total PP, despite lower phytoplankton growth rates, because of an increase in the productive water volume (Figure 1, right panels, and Figure 2a). Lastly, our experiments contribute to an understanding of

how changes in MLD can alter the carbon export. As expected, phytoplankton size composition was crucial to controlling carbon export (Figures 3a and 3b). Under conditions of deep winter mixed-layers and iron-rich environments, decreasing the MLD resulted in a reduction of the export by decreasing iron-supply and the presence of fast-sinking large phytoplankton. However, this trend reversed within environments dominated by small phytoplankton and export increased with decreasing mixed-layers. Two combined mechanisms likely controlled this trend. In the first place, a larger portion of PP was grazed by zooplankton (Figure 2d); hence, more organic matter could be exported as sinking particles in form of fecal pellets. In the second place, the shallower the mixed layer, the easier for particles to escape from surface turbulence and sink into the ocean (Palevsky & Doney, 2018).

These results have consequences on how we understand current and future SO productivity and export. First, because the iron distribution and winter mixed layer in the SO are zonally asymmetric (Tagliabue et al., 2014), future trends in PP and export are also likely to vary in both latitude and longitude. This conclusion agrees with the observed zonal asymmetries of phytoplankton phenology provinces (Ardyna et al., 2017) and challenges the prevailing latitudinal pattern of PP trends projected by most CMIP5 models (Bopp et al., 2013; Leung et al., 2015). We conclude that the latter is more likely to be caused by the inability of current climate models to correctly reproduce the zonal asymmetries in MLD (Sallée et al., 2010, 2013) and iron distribution (Schourup-Kristensen, 2015; Tagliabue et al., 2016). Second, the nonmonotonic response of PP to MLD should be further explored, particularly in observations, in order to evaluate the threshold depth in winter MLD within contrasted bioregions and identify which ecosystems are closer to collapse. Along this line, Ardyna et al. (2017) estimated an average threshold depth over the whole SO of ~150 m (their Figure S2) that can be used as a benchmark for future studies. From a modeling perspective, evaluating the evolution of trends by decade, instead of just comparing two extreme decades (i.e., projected against historical) may help elucidate the nonmonotonic responses in CMIP projections. Lastly, summer results suggest that changes in summer MLD do not significantly affect iron supply because the ferricline depth is always deeper than the deepest plausible range of climatological summer MLD (see Figure 1c in Tagliabue et al., 2014, which shows that the ferricline depth is deeper than 200 m over 75% of the observed summer iron profiles). Summer storms, however, which have not been accounted for in this study, may be more effective in supplying iron in the case of deeper summer MLDs (Carranza & Gille, 2015; Nicholson et al., 2016).

There are a number of assumptions in our modeling approach that should be kept in mind for future comparisons against observations or more complex models. First, we did not account for silicate limitation. The latter is the main limiting factor for diatoms during late summer in Sub-Antarctic waters of the SO (Leblanc et al., 2005). Changes in summer MLD might have a role on resupplying silicate and alter diatoms summer production. Second, the biogeochemical model used here simulates iron remineralization in a simplistic way (Aumont & Bopp, 2006). In our analysis we did not detect any significant change in summer iron concentration associated to remineralization. But it is possible that the representation of this mechanism in our model is too simplistic, because remineralization has been identified as a significant source of iron during summer in the SO (Tagliabue et al., 2014, 2017). How changes in summer MLD influence remineralization is out of scope of the current study but together with silicate limitation, these mechanisms could either compensate or intensify the summer trends presented here. Third, we made the choice to not consider changes in incoming solar radiation and used clear-sky conditions at 45°S latitude in all our experiments. At higher latitudes, where incoming solar radiation is lower, we would expect to find shallower threshold depths, although this could be compensated by higher iron demand by phytoplankton. More difficult is to anticipate the impacts of a nonclear-sky over phytoplankton growth, as incoming solar radiation is simultaneously influenced by seasonal and intraseasonal variability of cloud coverage, typology of clouds (type and altitude in the atmosphere), and sea-state (surface waves and bubbles). Fourth, we considered changes in MLD, but we did not take into account the associated changes in temperature and wind stress. The former is particularly interesting, as laboratory experiments have recently shown interactive effects between iron and temperature for SO diatoms (Hutchins & Boyd, 2016). Last, our study is based on a biogeochemical model that, despite its complexity, remains a simplification of the processes regulating phytoplankton growth. For instance, community structure was only represented in terms of size, but it is well known that different phytoplankton species of similar sizes respond differently to environmental changes (Arrigo et al., 1999). Also, our model did not account for the potential contribution of vertically migrating zooplankton and small nekton to the



carbon export. We should note however that despite these assumptions, the relationships between PP and MLD that came out of this modeling study are consistent with that suggested from in situ observations (Ardyna et al., 2017; Hoppe et al., 2017). Moreover, the analysis of a large ensemble of simulations also supports the robustness of our conclusions.

In conclusion, the results presented here provide a new and more refined explanation of the influence of MLD over SO PP and export. They provide a framework to analyze current and future patterns of production and export, in particular for CMIP6 projections and multiannual time series obtained from in situ observations such as moorings or BGC-Argo floats.

### Acknowledgments

We thank Laurent Bopp, Christian Ethé, Julien LeSommer, and Olivier Aumont for the technical support and insightful comments that strongly benefited this study. We also thank the two anonymous reviewers who took the time to review this work. We would like to acknowledge support from Sorbonne Université through the project PERSU. This study also benefited from the staff-exchange project SOCCLI, funded by EU (FP7-PEOPLE-2012-IRSES) and the SOBUMS project, funded by the Agence Nationale de la Recherche (ANR-16-CE01-0014). This research was supported under Australian Research Council's Special Research Initiative for Antarctic Gateway Partnership (Project ID SR140300001). The ensemble of model outputs used in this study can be freely accessed at <https://metadata.imas.utas.edu.au/geonetwork/srv/eng/main.home>, and the PISCES code specific for the model configuration used in this study is available at <https://github.com/jllort>.

### References

- Ardyna, M., Claustre, H., Sallée, J.-B., D'Ovidio, F., Gentili, B., van Dijken, G., et al. (2017). Delineating environmental control of phytoplankton biomass and phenology in the Southern Ocean: Phytoplankton dynamics in the SO. *Geophysical Research Letters*, *44*, 5016–5024. <https://doi.org/10.1002/2016GL072428>
- Arrigo, K. R., Robinson, D. H., Worthen, D. L., Dunbar, R. B., DiTullio, G. R., VanWoert, M., & Lizotte, M. P. (1999). Phytoplankton community structure and the drawdown of nutrients and CO<sub>2</sub> in the Southern Ocean. *Science*, *283*(5400), 365–367. <https://doi.org/10.1126/science.283.5400.365>
- Aumont, O., & Bopp, L. (2006). Globalizing results from ocean in situ iron fertilization studies. *Global Biogeochemical Cycles*, *20*, GB2017. <https://doi.org/10.1029/2005GB002591>
- Bopp, L., Resplandy, L., Orr, J. C., Doney, S. C., Dunne, J. P., Gehlen, M., et al. (2013). Multiple stressors of ocean ecosystems in the 21st century: Projections with CMIP5 models. *Biogeosciences*, *10*(10), 6225–6245. <https://doi.org/10.5194/bg-10-6225-2013>
- Boyd, P. W., Strzepek, R., Fu, F., & Hutchins, D. A. (2010). Environmental control of open-ocean phytoplankton groups: Now and in the future. *Limnology and Oceanography*, *55*(3), 1353–1376. <https://doi.org/10.4319/lo.2010.55.3.1353>
- Boyd, P. W., & Trull, T. W. (2007). Understanding the export of biogenic particles in oceanic waters: Is there consensus? *Progress in Oceanography*, *72*(4), 276–312. <https://doi.org/10.1016/j.pocean.2006.10.007>
- Bracegirdle, T. J., Shuckburgh, E., Sallée, J. B., Wang, Z., Meijers, A. J. S., Bruneau, N., et al. (2013). Assessment of surface winds over the Atlantic, Indian and Pacific Ocean sectors of the southern hemisphere in CMIP5 models: Historical bias, forcing response, and state dependence. *Journal of Geophysical Research: Atmospheres*, *118*, 547–562. <https://doi.org/10.1002/jgrd.50153>
- Cai, W., Shi, G., Cowan, T., Bi, D., & Ribbe, J. (2005). The response of the southern annular mode, the East Australian Current, and the southern mid-latitude ocean circulation to global warming. *Geophysical Research Letters*, *32*, L23706. <https://doi.org/10.1029/2005GL024701>
- Carranza, M. M., & Gille, S. T. (2015). Southern Ocean wind-driven entrainment enhances satellite chlorophyll-a through the summer. *Journal of Geophysical Research: Oceans*, *120*, 304–323. <https://doi.org/10.1002/2014JC010203>
- Cisewski, B., Volker, H. S., & Hartmut, P. (2005). Upper-ocean vertical mixing in the Antarctic Polar Front Zone. *Deep Sea Research Part II: Topical Studies in Oceanography*, *52*(9), 1087–1108. <https://doi.org/10.1016/j.dsr2.2005.01.010>
- Deppeler, S. L., & Davidson, A. T. (2017). Southern Ocean phytoplankton in a changing climate. *Frontiers in Marine Science*, *4*. <https://doi.org/10.3389/fmars.2017.00040>
- Doney, S. C. (2006). Oceanography: Plankton in a warmer world. *Nature*, *444*(7120), 695–696. <https://doi.org/10.1038/444695a>
- Hauck, J., Völker, C., Wolf-Gladrow, D. A., Laufkötter, C., Vogt, M., Aumont, O., et al. (2015). On the Southern Ocean CO<sub>2</sub> uptake and the role of the biological carbon pump in the 21st century. *Global Biogeochemical Cycles*, *29*, 1451–1470. <https://doi.org/10.1002/2015GB005140>
- Henson, S. A., Yool, A., & Sanders, R. (2015). Variability in efficiency of particulate organic carbon export: A model study. *Global Biogeochemical Cycles*, *29*, 33–45. <https://doi.org/10.1002/2014GB004965>
- Hoppe, C. J. M., Klaas, C., Ossebaar, S., Soppa, M. A., Cheah, W., Laglera, L. M., et al. (2017). Controls of primary production in two phytoplankton blooms in the Antarctic Circumpolar Current. *Deep Sea Research Part II: Topical Studies in Oceanography*, *138*, 63–73. <https://doi.org/10.1016/j.dsr2.2015.10.005>
- Hutchins, D. A., & Boyd, P. W. (2016). Marine phytoplankton and the changing ocean Iron cycle. *Nature Climate Change*, *6*(12), 1072–1079. <https://doi.org/10.1038/nclimate3147>
- Jeandel, C., Ruiz-Pino, D., Gjata, E., Poisson, A., Brunet, C., Charriaud, E., et al. (1998). KERFIX, a time-series station in the Southern Ocean: A presentation. *Journal of Marine Systems*, *17*(1–4), 555–569. [https://doi.org/10.1016/S0924-7963\(98\)00064-5](https://doi.org/10.1016/S0924-7963(98)00064-5)
- Laufkötter, C., Vogt, M., Gruber, N., Aita-Noguchi, M., Aumont, O., Bopp, L., et al. (2015). Drivers and uncertainties of future global marine primary production in marine ecosystem models. *Biogeosciences*, *12*(23), 6955–6984. <https://doi.org/10.5194/bg-12-6955-2015>
- Laufkötter, C., Vogt, M., Gruber, N., Aumont, O., Bopp, L., Doney, S. C., et al. (2016). Projected decreases in future marine export production: The role of the carbon flux through the upper ocean ecosystem. *Biogeosciences*, *13*(13), 4023–4047. <https://doi.org/10.5194/bg-13-4023-2016>
- Leblanc, K., Hare, C. E., Boyd, P. W., Bruland, K. W., Sohst, B., Pickmere, S., et al. (2005). Fe and Zn effects on the Si cycle and diatom community structure in two contrasting high and low-silicate HNLC areas. *Deep Sea Research Part I: Oceanographic Research Papers*, *52*, 1842–1864. <https://doi.org/10.1016/j.dsr.2005.06.005>
- Lenton, A., & Matear, R. J. (2007). Role of the Southern Annular Mode (SAM) in Southern Ocean CO<sub>2</sub> uptake. *Global Biogeochemical Cycles*, *21*, GB2016. <https://doi.org/10.1029/2006GB002714>
- Leung, S., Cabré, A., & Marinov, I. (2015). A latitudinally banded phytoplankton response to 21st century climate change in the Southern Ocean across the CMIP5 model suite. *Biogeosciences*, *12*(19), 5715–5734. <https://doi.org/10.5194/bg-12-5715-2015>
- Lévy, M. (2015). Exploration of the critical depth hypothesis with a simple NPZ model. *ICES Journal of Marine Science*, *72*(6), 1916–1925. <https://doi.org/10.1093/icesjms/fsv016>
- Llort, J., Lévy, M., Sallée, J.-B., & Tagliabue, A. (2015). Onset, intensification, and decline of phytoplankton blooms in the Southern Ocean. *ICES Journal of Marine Science: Journal du Conseil*, *72*(6), 1971–1984. <https://doi.org/10.1093/icesjms/fsv053>
- Lovenduski, N. S., & Gruber, N. (2005). Impact of the Southern Annular Mode on Southern Ocean circulation and biology. *Geophysical Research Letters*, *32*, L11603. <https://doi.org/10.1029/2005GL022727>

- Nicholson, S.-A., Lévy, M., Llort, J., Swart, S., & Monteiro, P. M. S. (2016). Investigation into the impact of storms on sustaining summer primary productivity in the sub-Antarctic Ocean. *Geophysical Research Letters*, *43*, 9192–9199. <https://doi.org/10.1002/2016GL069973>
- Palevsky, H. I., & Doney, S. C. (2018). How Choice of Depth Horizon Influences the Estimated Spatial Patterns and Global Magnitude of Ocean Carbon Export Flux. *Geophysical Research Letters*, *45*, 4171–4179. <https://doi.org/10.1029/2017GL076498>
- Panassa, E., Völker, C., Wolf-Gladrow, D., & Hauck, J. (2018). Drivers of interannual variability of summer mixed layer depth in the Southern Ocean between 2002 and 2011. *Journal of Geophysical Research: Oceans*, *123*, 5077–5090. <https://doi.org/10.1029/2018JC013901>
- Pellichero, V., Sallée, J.-B., Schmidtko, S., Roquet, F., & Charrassin, J.-B. (2017). The ocean mixed layer under Southern Ocean sea-ice: Seasonal cycle and forcing. *Journal of Geophysical Research: Oceans*, *122*, 1608–1633. <https://doi.org/10.1002/2016JC011970>
- Sallée, J. B., Shuckburgh, E., Bruneau, N., Meijers, A. J. S., Bracegirdle, T. J., & Wang, Z. (2013). Assessment of Southern Ocean mixed-layer depths in CMIP5 models: Historical bias and forcing response. *Journal of Geophysical Research: Oceans*, *118*, 1845–1862. <https://doi.org/10.1002/jgrc.20157>
- Sallée, J. B., Speer, K. G., & Rintoul, S. R. (2010). Zonally asymmetric response of the Southern Ocean mixed-layer depth to the southern annular mode. *Nature Geoscience*, *3*(4), 273–279. <https://doi.org/10.1038/ngeo812>
- Sarmiento, J. L., Slater, R., Barber, R., Bopp, L., Doney, S. C., Hirst, A. C., et al. (2004). Response of ocean ecosystems to climate warming. *Global Biogeochemical Cycles*, *18*, GB3003. <https://doi.org/10.1029/2003GB002134>
- Schourup-Kristensen, V. (2015). Iron in the Southern Ocean: Spatial distribution and the effect on the phytoplankton. Bremen University, Alfred-Wegener-Institute. Retrieved from <http://epic.awi.de/38667/>
- Swart, N. C., Fyfe, J. C., Gillett, N., & Marshall, G. J. (2015). Comparing trends in the southern annular mode and surface westerly jet. *Journal of Climate*, *28*(22), 8840–8859. <https://doi.org/10.1175/JCLI-D-15-0334.1>
- Swart, N. C., Gille, S. T., Fyfe, J. C., & Gillett, N. P. (2018). Recent Southern Ocean warming and freshening driven by greenhouse gas emissions and ozone depletion. *Nature Geoscience*, *11*(11), 836–841. <https://doi.org/10.1038/s41561-018-0226-1>
- Tagliabue, A., Aumont, O., DeAth, R., Dunne, J. P., Dutkiewicz, S., Galbraith, E., et al. (2016). How well do global ocean biogeochemistry models simulate dissolved iron distributions? *Global Biogeochemical Cycles*, *30*, 149–174. <https://doi.org/10.1002/2015GB005289>
- Tagliabue, A., Bowie, A. R., Boyd, P. W., Buck, K. N., Johnson, K. S., & Saito, M. A. (2017). The integral role of iron in ocean biogeochemistry. *Nature*, *543*(7643), 51–59. <https://doi.org/10.1038/nature21058>
- Tagliabue, A., Mtshali, T., Aumont, O., Bowie, A. R., Klunder, M. B., Roychoudhury, A. N., & Swart, S. (2012). A global compilation of dissolved iron measurements: Focus on distributions and processes in the Southern Ocean. *Biogeosciences*, *9*(6), 2333–2349. <https://doi.org/10.5194/bg-9-2333-2012>
- Tagliabue, A., Sallée, J.-B., Bowie, A. R., Lévy, M., Swart, S., & Boyd, P. W. (2014). Surface-water iron supplies in the Southern Ocean sustained by deep winter mixing. *Nature Geoscience*, *7*(4), 314–320. <https://doi.org/10.1038/ngeo2101>
- Taylor, K. E., Stouffer, R. J., & Meehl, G. A. (2012). An overview of CMIP5 and the experiment design. *Bulletin of the American Meteorological Society*, *93*(4), 485–498. <https://doi.org/10.1175/BAMS-D-11-00094.1>
- Venables, H., & Moore, C. M. (2010). Phytoplankton and light limitation in the Southern Ocean: Learning from high-nutrient, high-chlorophyll areas. *Journal of Geophysical Research*, *115*, C02015. <https://doi.org/10.1029/2009JC005361>
- Zheng, F., Li, J., Clark, R. T., & Nnamchi, H. C. (2013). Simulation and projection of the southern hemisphere annular mode in CMIP5 models. *Journal of Climate*, *26*(24), 9860–9879. <https://doi.org/10.1175/JCLI-D-13-00204.1>